# The Spectral Dependence of the Optical Properties of Human Brain

H.J.C.M. STERENBORG [a, b], M.J.C. VAN GEMERT [a, b], W. KAMPHORST [c], J.G. WOLBERS [d], W. HOGERVORST [a]

[a] Laser Application and Information Centre, Amsterdam, Netherlands
[b] Experimental Laser Centre, Academic Hospital of the University of Amsterdam, Meibergdreef 9, 1105 AZ Amsterdam, Netherlands
[c] Division of Neuropathology, Department of Pathology, Free University Hospital, Amsterdam, Netherlands
[d] Department of Neurosurgery, Free University Hospital, Amsterdam, Netherlands
Correspondence to H.J.C.M. Sterenborg

**Abstract.** The in vitro optical properties of slices of human brain tissue were measured. The experiments were performed with an integrating sphere and covered the wavelength range from 400 to 1100 nm. Both normal brain tissue (white and grey matter) and tumour tissue (a malignant glioma and a melanotic melanoma) were investigated. From the experimental data the Kubelka–Munk absorption and scattering coefficients were determined. From these data we calculated the transport absorption and scattering coefficients by using the diffusion approximation. Blood and water appeared to be the dominant chromophores. In the wavelength range mentioned, the absorption coefficients varied over more than two orders of magnitude. The scattering coefficients increased slowly towards the shorter wavelengths.

## INTRODUCTION

The optical properties of human brain tissues have, so far, only been studied in relation to photodynamic therapy (1–5). That is, only the attenuation coefficient and fluence-rate distributions have been measured under in vivo and in vitro conditions at the limited number of wavelengths at which lasers are available. Recently, interstitial irradiation of brain tumours by stereotactically placed fibres has been suggested as an interesting neurosurgical development in treating brain malignancies. Optimal laser parameters for this treatment are lacking so far. A full appreciation of the physical basis of this treatment requires information on the resulting fluence-rate distribution in the tissue, the thermal properties and the biological response. In the present paper we present measurements of the optical parameters as a function of wavelength in a wide spectral region: 400–1100 nm.

## MATERIALS AND METHODS

### Tissue

Slices of human brain tissue were investigated: white matter, grey matter, a melanotic melanoma and a malignant glioma (Table 1). The thickness of the slices varied between 1.4 and 5.8 mm. The measurements on the glioma were performed 4 h after surgery. All other samples were obtained from autopsies and processed within 24 to 36 h post-mortem.

### Technique

Transmission and reflection of each tissue sample was measured using an integrating sphere. The sphere had an internal diameter of 11 cm. Its internal surface was painted with Kodak High Reflectance Coating. The sphere was constructed at the St. Joseph Hospital in Eindhoven by R.M. Verdaasdonk (unpublished). The outlines of the experimental set-up are shown in Fig. 1. The light source used was a 100 W Xenon arc lamp. The radiation produced was filtered through a monochromator with a spectral bandwidth of 4 nm. The outcoming light was coupled into the sphere with a small lens, in order to spread the light over the sphere's internal surface. The tissue was placed in the sample holder and kept in position by two thin glass sheets (thickness 160 $\mu$m). The sheets were

Paper received August 1989

*Table 1.* Specifics of the different samples

| Sample number | Type of tissue | Sample thickness (mm) | Sex | Age (years) | |
|---|---|---|---|---|---|
| 1a | white matter | 2.3 | F | 32 | 24 h post mortem |
| 1b | white matter | 4.0 | | | |
| 1c | white matter | 5.8 | | | |
| 2a | white matter | 2.0 | F | 63 | 30 h post mortem |
| 2b | white matter | 3.0 | | | |
| 2c | white matter | 4.1 | | | |
| 3a | grey matter | 1.4 | M | 71 | 24 h post mortem |
| 3b | grey matter | 2.0 | | | |
| 3c | grey matter | 4.9 | | | |
| 4a | glioma | 2.0 | M | 65 | 4 h post operative |
| 5a | melanoma | 1.3 | M | 71 | 24 h post mortem |
| 5b | melanoma | 4.0 | | | |

parallel mounted and at a fixed distance apart measured with a micrometer. A few drops of saline were added to avoid sample dehydration. Reflected and transmitted radiation were detected with Silicon photodiodes (BPW 34) using standard lock-in techniques. The wavelength was scanned from 400 to 1100 nm. Three different scans were made: one with sample, one with a reflectance standard in the sample holder and one with an empty sample holder. The reflection ($R$) and transmission ($T$) coefficients were then calculated by using the following equations.

$$T = T_{\text{ref}} \frac{t_s - t_0}{t_r - t_0} \tag{1}$$

and

$$R = R_{\text{ref}} \frac{r_s - r_0}{r_r - r_0} \tag{2}$$

where $t$ and $r$ stand for the measured values of transmission and reflection and the subscripts $s$, $r$ and 0 refer to the sample, the reflectance standard and the empty sample holder, respectively. $T_0$ appeared to be negligible in all cases, $T_{\text{ref}}$ and $R_{\text{ref}}$ stand for the reference transmission and reflection values (100%, empty sample holder, and 85%, reflectance standard, respectively).

## Data analysis

The change in refractive index at the tissue boundaries causes reflections. A correction for internal and external reflections was made by using the relations derived by Kottler (5).

$$R_m = r_e + (1 - r_e)(1 - r_e)(R_d - r_i R_d^2 + r_i T_d^2)/D, \tag{3}$$

$$T_m = T_d(1 - r_e)(1 - r_i)/D, \tag{4}$$

where

$$D = (1 - r_i R_d)^2 - r_i^2 T_d^2, \tag{5}$$

and $T_m$, $R_m$, $T_d$ and $R_d$ stand for the measured transmission value, the measured reflection value, the volume transmision and the volume reflection, respectively. The parameters $r_e$ and $r_i$ are the coefficients of external and internal reflection. Assuming perfectly diffuse radiation and a refractive index of $n = 1.5$, we calculated: $r_e = 0.09$ and $r_i = 0.56$. Calculation of the volume transmission and reflection from the measured transmission and reflection is straightforward and shown in Appendix A.

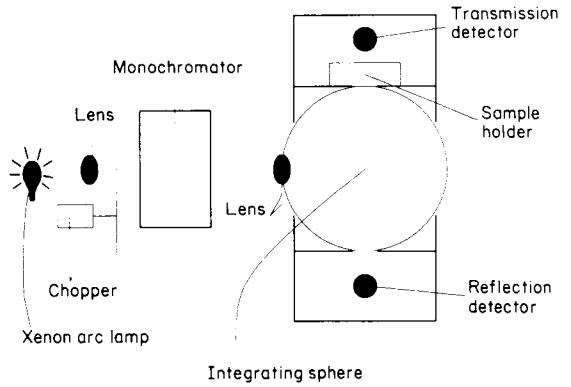


*Fig. 1.* The experimental set-up.

From the corrected volume transmission and reflection we derived the Kubelka–Munk (KM) absorption, $A_{km}$, and scattering, $S_{km}$, coefficients using the following relations (7):

$$S_{km} = \ln\left[\frac{1 - R_d(a-b)}{T_d}\right] \Big/ bx \qquad (6)$$

$$A_{km} = S_{km}(a-1) \qquad (7)$$

with

$$a = \frac{1 + R_d^2 - T_d^2}{2R_d} \qquad b = (a^2-1)^{\frac{1}{2}} \qquad (8), (9)$$

and where $x$ stands for the sample thickness.

The transport absorption $-,\sigma_a$, and reduced scattering coefficients, $\sigma_s(1-g)$, were derived from the Kubelka–Munk parameters $a_{km}$ and $S_{km}$ by using the relations derived by van Gemert & Star (8):

$$A_{km} = \frac{2\sigma_a}{1 + \sigma_a/\{2[\sigma_a + \sigma_s(1-g)]\}} \qquad (10)$$

$$S_{km} = \frac{\frac{3}{4}\sigma_s(1-g)}{1 + 19\sigma_a/\{30[\sigma_a + \sigma_s(1-g)]\}} \qquad (11)$$

The parameter $g$ is the anisotropy factor. It is defined as the mean cosine of the scattering angle. The parameters $\sigma_s$ and $g$ cannot be determined separately from diffuse measurements only. Hence, we are limited to the use of the reduced scattering coefficient $\sigma_s(1-g)$. The derivation of the inverse relations is given in Appendix B.

## RESULTS

Transmission and reflection as a function of wavelength and corrected for internal and external reflections are plotted in Fig. 2(a)–(d).

The Kubelka–Munk absorption coefficients $A_{km}$ for samples 1 to 4 are shown in Fig. 3(a). The data for sample 5, the melanoma, are shown in Fig. 5. The values were calculated using eqs 6 to 11 and the sample thickness $x$. The curves drawn represent values averaged over several samples of different thicknesses.

The Kubelka–Munk scattering coefficients, $S_{km}$, also calculated using eqs 6 to 11, for samples 1 to 5 are shown in Fig. 3(b).

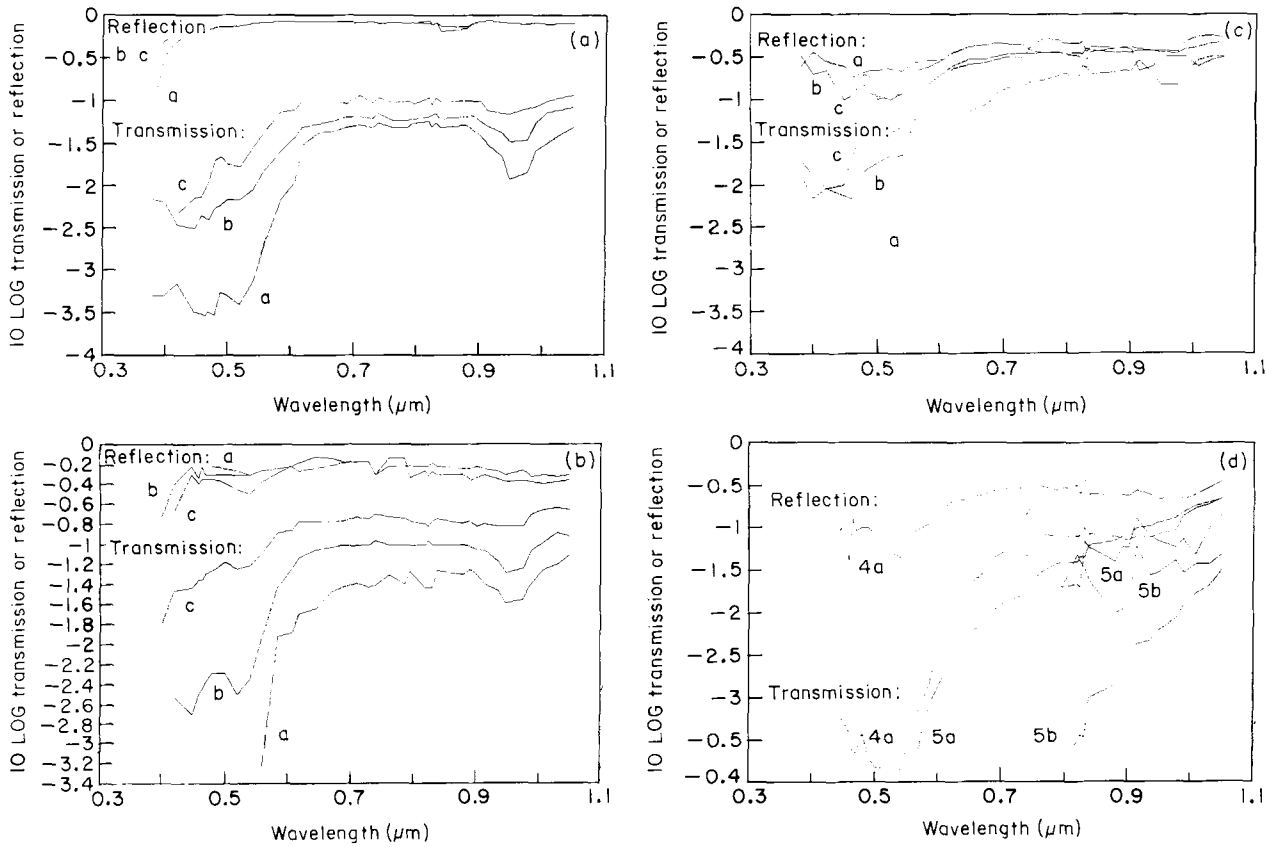


*Fig. 2.* Transmission, $T$, and reflection, $R$, of samples 1 to 5: (a) sample 1 (white matter); (b) sample 2 (white matter); (c) sample 3 (grey matter); (d) samples 4 and 5 (glioma and melanoma). The indices a, b and c in the graphs refer to the individual samples.

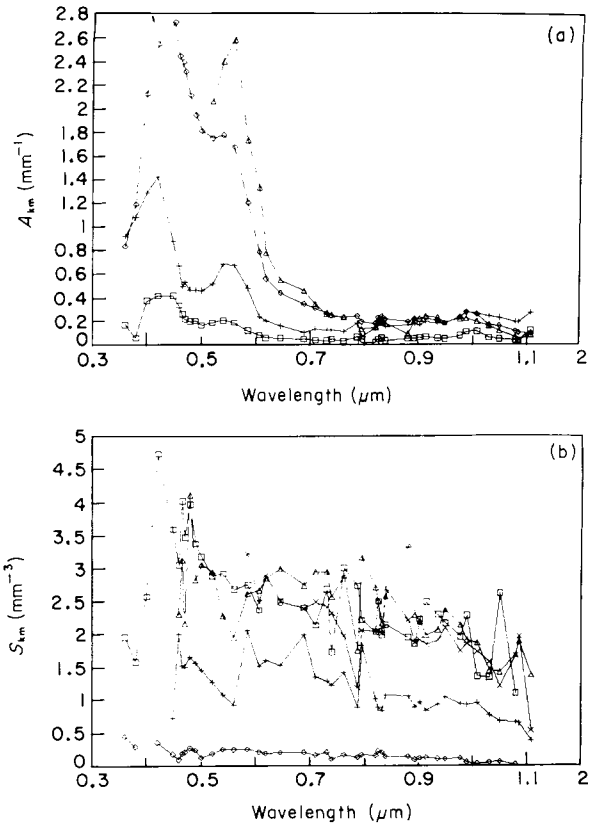


*Fig. 3.* (a) The Kubelka–Munk absorption coefficients, $A_{km}$, for samples 1 to 4 and (b) the Kubelka–Munk scattering coefficients, $S_{km}$, for samples 1 to 5. □ sample 1 (white matter); + sample 2 (white matter); ◇ sample 3 (grey matter); △ sample 4 (glioma); × sample 5 (melanoma).

The transport absorption coefficient, $\sigma_a$, for samples 1 to 4 are shown in Fig. 4(a) and the data for sample 5, the melanoma, in Fig. 5. The values were calculated using eqs 10 to 12 and the data shown in Figs 3(a), 3(b) and 5.

The transport scattering coefficients, $\sigma_s(1 - g)$, for samples 1 to 4, are shown in Fig. 4(b). Again, the values were calculated using eqs 10, 11 and 12 and the data shown in Figs 3(a), 3(b) and 5.

## DISCUSSION

### Absorption

The curve of the absorption coefficient of the melanoma closely matches the curve of the molar extinction coefficient of melanin (9), which is not surprising. The other absorption curves, Figs 3(a) and 4(a), show large differences for the different samples and tissue types used. However, the overall shape of these curves is rather similar: high absorption at wavelengths below 450 nm, a broad peak around 560 nm, less absorption in the range from 700 to 900 nm, with a minimum around 800 nm and a broad peak around 1000 nm. This behaviour strongly suggests that (anoxic) blood and water are the main absorbers in healthy brain tissue. The large quantitative variations between the coefficients of the different tissues in the region from 400 to 800 nm may be due to variations in the blood content of the different samples. Such variations could reflect a realistic difference between different types of tissue. For instance the malignant glioma sample was significantly more vascularized than the other samples. For

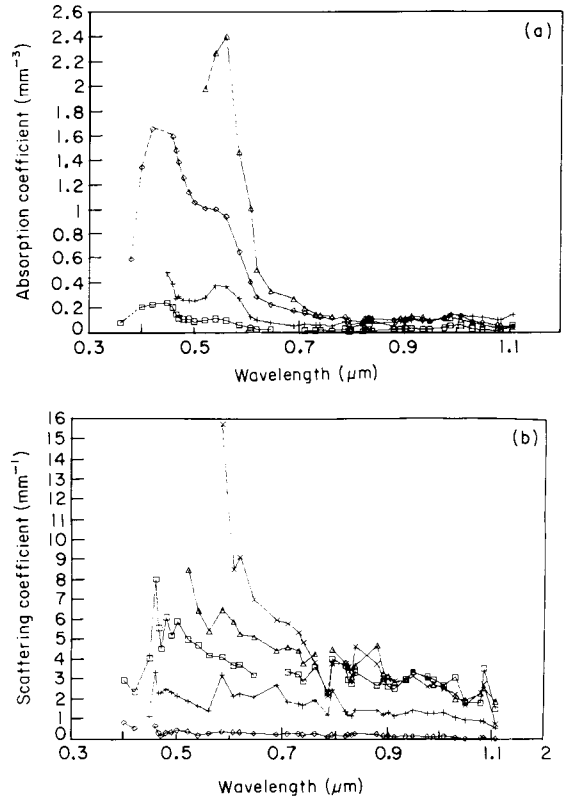


*Fig. 4.* (a) The transport absorption coefficients, $\sigma_a$, for samples 1 to 4 and (b) the transport scattering coefficients, $\sigma_s$, for samples 1 to 5. □ sample 1 (white matter); + sample 2 (white matter); △ sample 3 (grey matter); ◇ sample 4 (glioma); × sample 5 (melanoma).

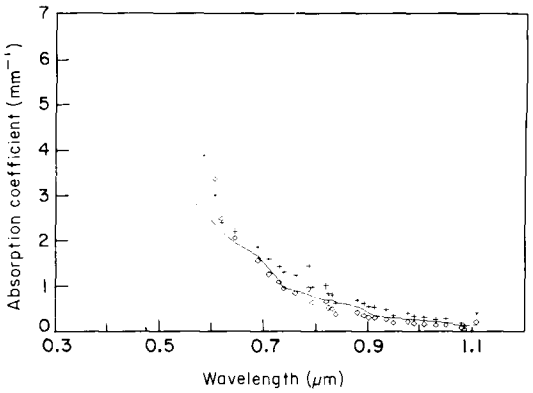


the samples of healthy grey and white matter it is more likely that variations in the blood content were caused by blood leakage due to mechanical stress on the tissue during resection and preparation for measurement. As a consequence, the in vivo blood content will probably be higher and thus the in vivo absorption coefficient will be higher than reported in the wavelength range from 400 to 600 nm. Another point is that in an in vivo situation, oxygen will be bound to the blood. This will alter the absorption data accordingly. Sample number 1 (Table 1) was taken from a patient who had suffered from a liver disease. The brain of this person showed a slight yellowish colour. This may have influenced the optical parameters.

## Scattering

The scattering coefficients $S_{km}$ and $\sigma_s(1-g)$ are plotted in Figs 3(b) and 4(b), for all samples. Again, differences between the various samples are apparent. Still, the glioma and melanoma tissue show scattering coefficients that are slightly larger than the others, over the whole wavelength range. The shapes of the curves are rather similar to what was found for other types of living tissue [i.e. dermis (10)]. The rather small variation of the scattering coefficient with wavelength suggests Mie scattering (11), i.e. scattering by particles much larger than the wavelength.

*Fig. 5.* The Kubłka–Munk absorption coefficient, $A_{km}$, the transport absorption coefficient, $\sigma_a$, and, for comparison, the absorption coefficient of melanin in arbitrary units. ◇ transport absorption coefficient ($mm^{-1}$); + Kubelka–Munk absorption coefficient ($mm^{-2}$); — absorption coefficient of melanin (in arbitrary units).

## Penetration depth

The diffusion model characterizes the light distribution in a scattering medium using two parameters: a diffusion constant and a penetration depth. A number of investigators have analysed their measurements on human brain tissue and calculated penetration depths for various wavelengths (2–4). To be able to compare the present results with the outcome of their experiments, we will calculate penetration depths from our results using (11).

$$\delta = [3\sigma_a(\sigma_a + \sigma_s(1-g)]^{-\frac{1}{2}} \qquad (15)$$

where $\delta$ stands for the penetration depth. This analysis is valid in the cases scattering dominate absorption, which seems a reasonable assumption here in view of the results shown in Fig. 4. Penetration depths calculated in this way, together with the values from the literature, are shown in Fig. 6. The differences are rather large, but not larger than the variations observed within the various experiments.

# CONCLUSIONS

## Tumour treatment

For the treatment of brain tumours with light, two options are available: hyperthermia (i.e. selective tumour-cell destruction induced by

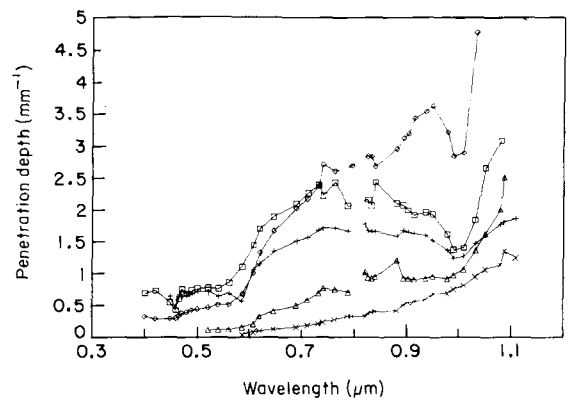


*Fig. 6.* The optical penetration depth, $\delta$, for samples 1 to 5, calculated with eq. (15) and based on the data shown in Figs 4(a) and (b).

temperatures in the range of 42 °C to 45 °C) and photodynamic therapy (i.e. selective tumour-cell destruction using tumour-selective photosensitizers). For the treatment of bulky tumours, both therapies desire a maximum penetration of the optical radiation into both healthy and tumour tissue. Figure 6 shows that maximum penetration into both healthy and tumorous brain tissue is reached between 1050 and 1100 nm. This suggests the use of an Nd-YAG laser.

Most photosensitizers presently in use for photodynamic therapy or under investigation operate at wavelengths between 625 and 800 nm. For the treatment of an area which contains a relatively small percentage of tumour tissue (e.g. the tumour bed remaining after resection of the main tumour mass), the wavelength range from 700 to 900 nm is equally as suitable as 1060 nm. However, for the treatment of bulky tumours again the Nd-YAG laser wavelength seems to be superior to the 700 to 900 nm wavelength range. Maeda et al (12) used the photosensitizer pheophorbide-a for PDT of rat skin tumours. This photosensitizer responds to the 1060 nm output of the Nd-YAG laser. At present this substance is not available for clinical use, but this may change in the future.

A relatively new development in laser technology are the high-power semiconductor lasers. These lasers emit in the wavelength range around 820 nm and deliver up to 1 W of optical power into a fibre. Figure 6 shows that radiation of this wavelength can penetrate up to 3 mm into healthy brain tissue. A hyperthermia system using this type of laser would be relatively simple and cheap.

## APPENDIX A

Into the formulae of Kottler (eqs 3 to 5) we substitute:

$$X = 1 - r_i R_d, \tag{A1a}$$

$$Y = r_i T_d, \tag{A1b}$$

$$Z = \frac{(1 - r_i)(1 - r_e)}{r_i}. \tag{A1c}$$

Hence, we find:

$$R_m = r_e + \frac{Z[X(1 - X) + Y^2]}{(X^2 - Y^2)}, \tag{A2a}$$

$$T_m = \frac{ZY}{(X^2 - Y^2)}. \tag{A2b}$$

Straightforward analysis yields

$$(X^2 - Y^2)(R_m - r_e + Z) = XZ, \tag{A3a}$$

$$(X^2 - Y^2)T_m = YZ. \tag{A3b}$$

Rearranging eq. (A3a) gives

$$X = \frac{Y(R_m - r_e + Z)}{T_m}, \tag{A4}$$

or $X = uY$, with

$$u = \frac{(R_m - r_e + Z)}{T_m}. \tag{A5}$$

Substitution of eq. A5 into A3b yields

$$Y = \frac{(u^2Y^2 - Y^2)}{T_m} \tag{A6}$$

which can be solved simply leading to

$$Y = \frac{Z}{T_m(u^2 - 1)}, \tag{A7a}$$

combining this with eq. A5 yields

$$X = \frac{Zu}{T_m(u^2 - 1)} \tag{A7b}$$

Using eq. A1, we derive the formulae for $T$ and $R$:

$$R_d = \frac{1}{r_i} \frac{Zu}{r_i T_m(u^2 - 1)}, \tag{A8a}$$

$$T_d = \frac{Z}{r_i T_m(u^2 - 1)}, \tag{A8b}$$

where $u$ can be found using eq. A1c and A5.

## APPENDIX B

The formulae linking $A_{km}$ and $S_{km}$ with $\sigma_a$ and $\sigma_s$ derived by van Gemert et al (9) are

$$A_{km} = \frac{2\sigma_a}{1 + \sigma_a/2[\sigma_a + \sigma_s(1 - g)]}, \tag{B1a}$$

$$S_{km} = \frac{\frac{3}{4}\sigma_s(1 - g)}{1 + 19\sigma_a/30[\sigma_a + \sigma_s(1 - g)]}. \tag{B1b}$$

In order to derive the inverse relations between $\sigma_a$, $\sigma_s(1 - g)$ and $A_{km}$, $S_{km}$, we define $p$ as

$$p = \frac{\sigma_a}{\sigma_a + \sigma_s(1 - g)}. \tag{B2}$$

Substitution of eq. (B2) into (B1) leads to

$$\sigma_a = \frac{A_{km}(1 + p/2)}{2}, \quad \text{(B3a)}$$

$$\sigma_s(1 - g) = \tfrac{4}{3}S_{km}(1 + \tfrac{19}{30}p); \quad \text{(B3b)}$$

$p$ can be derived by substituting eq. (B3) into (B2). We then get a quadratic equation in $p$ which can be solved easily. Only the positive root is valid, as $p \geq 0$

$$p = \frac{-(\tfrac{4}{3}S_{km} + A_{km}/4)}{2(A_{km}/4 + \tfrac{76}{90}S_{km})}$$

$$+ \frac{\sqrt{(\tfrac{4}{3}S_{km} + A_{km}/4)^2 + 2A_{km}(A_{km}/4 + \tfrac{76}{90}S_{km})}}{2(A_{km}/4 + \tfrac{76}{90}S_{km})}. \quad \text{(B4)}$$

## REFERENCES


1 Muller PJ, Wilson B. Photodynamic therapy of malignant primary brain tumors: clinical effects, post operative ICP, and light penetration of the brain. *Photochem Photobiol* **5**:929–35

2 Svaasand LO, Ellingsen R. Optical properties of human brain. *Photochem Photobiol* 1983, **38**:293–99

3 Muller PJ, Wilson BC. An update on the penetration depth of 630 nm light in normal and malignant human brain tissue in vivo. *Phys Med Biol* 1986, **31**:1295–7

4 Wilson BC, Patterson MS, Burns DM. The effect of photosensitiser concentration on the penetration depth of photoactivating light. *Lasers Med Sci* 1986, **1**:235–44

5 Powers S, Brown JT. Light dosimetry in brain tissue: an in-vivo approach, applicable to photodyamic therapy. *Lasers Surg Med* 1986, **6**:318–40

6 Kottler F. Turbid media with plane parallel surfaces. *J Opt Soc Am* 1960, **50**:483–90

7 van Gemert MJC, Hulsbergen-Henning JP. A model approach to laser coagulation of dermal vascular lesions. *Arch Dermatol Res* **270**:429–39

8 van Gemert MJC, Star WM. Relations between the Kubelka–Munk and the transport equation models for anisotropic scattering. *Laser Life Sci* 1987, **1**:27–98

9 Arndt K, Noe J, Rosen S. *Cutaneous laser therapy, principles and methods*. New York: John Wiley 1983

10 Anderson RR, Parrish JA. The optics of human skin. *J Invest Dermatol* 1983, **77**:13–19

11 Ishimaru A. Wave propagation and scattering in random media. New York: Academic Press 1978

12 Maeda N, Ichikawa K, Kobayashi T, Mizuno N. Pheophorbide-a photoradiation therapy for rat skin tumor. *Photomed Photobiol* 1984, **6**:7–11


*Key words:* Optical properties; Photodynamic therapy; Glioma; Brain tumour